Wide-Energy-Gap Host Materials for Blue Phosphorescent Organic Light-Emitting Diodes

Shanghui Ye,[†,‡] Yunqi Liu,*[,†] Chong-an Di,[†] Hongxia Xi,[†,‡] Weiping Wu,[†,‡] Yugen Wen,[†,‡] Kun Lu,[†,‡] Chunyan Du,[†,‡] Ying Liu,[†,‡] and Gui Yu[†]

Beijing National Laboratory for Molecular Sciences, Key Laboratory of Organic Solids, Institute of Chemistry, and Graduate School, Chinese Academy of Sciences, Beijing 100190, P. R. China

Received December 1, 2008. Revised Manuscript Received January 30, 2009

Two novel wide-energy-gap molecules, 1,3-bis(9-phenyl-9*H*-fluoren-9-yl)benzene (mDPFB) and 1,4-bis(9-phenyl-9*H*-fluoren-9-yl)benzene (pDPFB), suitable for blue phosphorescent host materials, were designed and prepared. The thermal, photophysical, and electrochemical properties as well as electroluminescence characteristics were fully investigated. Both mDPFB and pDPFB possess high singlet (4.0 eV) and triplet (2.8 eV) energies, well energy-matched with the deep-blue phosphorescent dopant, iridium(III) bis(4′,6′-difluorophenylpyridinato)tetrakis(1-pyrazolyl)borate (FIr6). The single crystals of the newly synthesized compounds mDPFB and pDPFB were grown, and their crystal structures were determined by X-ray diffraction. Both molecules adopt a rigid twisted tetrahedral crystallographic conformation, and no facial to facial $\pi-\pi$ stacking exists in the solid state. The substituents at the 1,4-positions of benzene enhance the twisted degree of the fluorenyl rings and have predominant influence on the thermal and morphological properties. Both molecules possess excellent thermal stability with decomposition temperatures (T_d) of 354 and 386 °C in nitrogen, respectively. Blue phosphorescent organic light-emitting diodes (OLEDs) were fabricated using pDPFB or mDPFB as host materials and FIr6 as a blue phosphorescent dopant with the configuration of ITO/NPB/mCP/host:FIr6/BCP/Ca:Ag. Devices based on the pDPFB host showed a maximum luminous power efficiency of 18.9 lm/W, with CIE coordinates (x, y) of (0.18, 0.33), improved by a factor of over 10 compared with the reference devices based on *N*,*N*′-dicarbazolyl-3,5-benzene (mCP) host. We discussed the mechanism and demonstrated that highly efficient blue phosphorescent OLEDs can be achieved in designing host materials which possess matched energy levels with the phosphorescent dopant, with high miscibility to the dopant, and with excellent film-forming ability and thermal and morphological stability.

Introduction

During the past decade, organic light-emitting devices (OLEDs) have made dramatic progress; high brightness and efficiency and lifetimes greater than 10 000 h have been achieved for green and red light-emitting diodes, which have already approached or even exceeded the requirement of a practical application.[1−7] The development of high-performance material is of the key importance for the fabrication of high-performance OLEDs. Efficient and stable blue OLEDs, however, remain a challenge. Most of the highly efficient blue OLEDs are based on phosphorescent materials; among them, bis[2-(4′,6′-difluorophenyl)pyridinato-N,C$^{2'}$]-iridium(III) picolinate (FIrpic) is the most popular choice. However, FIrpic is a sky-blue emitter, with an emitting peak at 472 nm. Another promising blue phosphorescent material of practical use may be iridium(III) bis(4′,6′-difluorophenylpyridinato)tetrakis(1-pyrazolyl)borate (FIr6), whose emission centered at 460 nm and blue-color chromaticity had been considerably improved to $CIE_{x,y} = (0.16, 0.26)$.[8] Furthermore, in recently reported work on the use of 1,1-bis[(di-4-tolylamino)phenyl]cyclohexane as a hole-transporting and electron-blocking layer in FIr6-based deep-blue phosphorescent OLEDs, Zheng et al. achieved a maximum external quantum efficiency of η_{EQE} (18 ± 1)%.[9]

However, authentic blue-emitting phosphorescent OLEDs remain rare, which is attributed to the failure in designing suitable host material and the accompanying pure blue phosphor. In principle, a good host material must meet the following requirements: (1) its triplet energy must be higher than that of the guest molecule to prevent reverse energy transfer and to efficiently confine triplet exciton on the guest

* Corresponding author. E-mail: liuyq@iccas.ac.cn.
† Institute of Chemistry.
‡ Graduate School of Chinese Academy of Sciences.

(1) Forrest, S. R. *Nature* **2004**, *428*, 911.
(2) He, G. F.; Pfeiffer, M.; Leo, K.; Hofmann, M.; Birnstock, J.; Pudzich, R.; Salbeck, J. *Appl. Phys. Lett.* **2004**, *85*, 3911.
(3) Ikai, M.; Tokito, S.; Sakamoto, Y.; Suzuki, T.; Taga, Y. *Appl. Phys. Lett.* **2001**, *79*, 156.
(4) Adachi, C.; Baldo, M. A.; Forrest, S. R.; Thompson, M. E. *Appl. Phys. Lett.* **2000**, *77*, 904.
(5) Tong, B. H.; Mei, Q. B.; Wang, S. J.; Fang, Y.; Meng, Y. Z.; Wang, B. *J. Mater. Chem.* **2008**, *18*, 1636.
(6) Adachi, C.; Baldo, M. A.; Thompson, M. E.; Forrest, S. R. *J. Appl. Phys.* **2001**, *90*, 5048.
(7) Kawamura, Y.; Goushi, K.; Brooks, J.; Brown, J. J.; Sasabe, H.; Adachi, C. *Appl. Phys. Lett.* **2005**, *86*, 077104.
(8) Holmes, R. J.; D'Andrade, B. W.; Forrest, S. R.; Ren, X.; Li, J.; Thompson, M. E. *Appl. Phys. Lett.* **2003**, *83*, 3818.
(9) Zheng, Y.; Eom, S. H.; Chopra, N.; Lee, J. W.; So, F.; Xue, J. G. *Appl. Phys. Lett.* **2008**, *92*, 223301.

10.1021/cm8032302 CCC: $40.75 © 2009 American Chemical Society
Published on Web 03/09/2009

molecules;[10,11] (2) it must possess good film-forming ability and chemical stability to extend the operational lifetime of the device. Such requirements become very difficult to achieve in blue phosphorescent devices because blue phosphors have a very high triplet energy and require that the corresponding host materials have a higher triplet energy to meet them, thus requiring wide energy gaps. This means that the host material must possess very short π-conjugation length to achieve a high triplet energy level, which negatively affects the charge carrier injection into the host materials and transport properties. There is a tradeoff between increasing the band gap of a material to increase singlet and triplet energies and decreasing the π-aromatic system, which may adversely affect charge transport properties.[12]

There are some reports of efficient blue-phosphorescent host material, such as substituting the fluorene chromophore with triphenylamine[13] or diphenylphosphine oxide,[12,14−16] carbazole/fluorene hybrids,[17,18] silane-modified 1,3-bis-(9-carbazolyl)-benzene,[19,20] poly(9,9-alkyl3,6-silafluorene),[21] and carbazole-pyridine.[22] The most reported blue phosphorescent host materials are carbazole-based materials or phenylsilanes;[8,19,23−29] however, carbazole-based materials have highest occupied molecular orbital (HOMO) levels of about 5.9 eV, which fall near or above the HOMO levels of FIr6 (6.1 eV), making them unsuitable for efficient carrier collection and recombination and ultimately limiting device efficiency.[30] As for the phenylsilanes, such as tetraphenylsilane functionalized ultrahigh energy gap hosts (UHGs), they have ultrawide HOMO to lowest unoccupied molecular orbital (LUMO) energy gaps (in the range of 4.5−5.0 eV), which serve as inert matrixes, leaving the guest molecules to both trap and conduct charge, allowing for direct excitonic formation on the guest phosphor, and leading to increased driving voltage and thus lower power efficiency.[8] The most desirable host seems to be a silane−fluorene hybrid,[31] whose HOMO level is at about 6.3 eV and whose LUMO is at 2.4 eV, which is below and above those of the FIr6 dopant, respectively.

In this paper, we report a novel route to synthesis of two new host materials—1,3-bis(9-phenyl-9*H*-fluoren-9-yl)benzene (mDPFB) and 1,4-bis(9-phenyl-9*H*-fluoren-9-yl)benzene (pDPFB)—for FIr6, the commercially available deep-blue phosphorescent emitter. The design concept is based on the fact that fluorene has both a large energy level of 2.89 eV[31] and high light-emitting efficiency. Given that the fluorene is connected to an inert core through the sp^3-hybridized carbon atom at the C-9 of the fluorene, which performs as a spacer to block extended π-conjugation, the conjugation length and triplet energy level of each individual building block in the resulting composite should remain unchanged. The resulting materials should maintain high triplet energy level and enhanced thermal and morphological stabilities. The synthesis and characterization of these new fluorenyl derivatives, including crystal structure, photophysical and electrochemical properties, surface morphology, and electroluminescence (EL) properties, are well presented. Devices based on pDPFB host and FIr6 phosphorescent emitter displayed intrinsically blue emission from the dopant with a maximum luminous power efficiency of 18.9 lm/W.

Experimental Section

Materials. All the solvents were distilled from appropriate drying agents prior to use. Commercially available reagents were used without further purification.

Measurements. ^{1}H NMR and ^{13}C NMR measurements were carried out on a Bruker DMX 400 NMR spectrometer. MS spectrometry (MALDI-TOF-MS) was determined on a Bruker BIFLEX III mass spectrometer. Elemental analyses were carried out on a Carlo-Erba 1160 elemental analyzer. Thermogravimetric analyses (TGA) were carried out using a Perkin-Elmer thermogravimeter (model TGA7) under a dry nitrogen gas flow at a heating rate of 10 °C/min. Glass transition temperatures (T_g) and melting phase-transition temperature (T_m) were determined by differential scanning calorimetry (DSC) at a heating rate of 10 °C/min using a Perkin-Elmer differential scanning calorimeter (DSC7). The voltammetric characterization of the redox process was performed with a computer-controlled CHI 600C Electrochemical Workstation using a Pt disk working electrode of 0.01 cm^2, a Pt wire counter electrode, and a Ag/AgCl reference electrode in a conventional three-electrode cell. X-Ray diffraction (XRD) measurements were carried out in the reflection system at RT using a Rigaku MM-007 X-ray diffraction system (Mo Kα radiation, $\lambda = 0.71073$ Å).

(10) Adachi, C.; Kwong, R. C.; Djurovich, P.; Adamovich, V.; Baldo, M. A.; Thompson, M. E.; Forrest, S. R. *Appl. Phys. Lett.* **2001**, *79*, 2082.
(11) Tanaka, I.; Tabata, Y.; Tokito, S. *Chem. Phys. Lett.* **2004**, *400*, 86.
(12) Padmaperuma, A. B.; Sapochak, L. S.; Burrows, P. E. *Chem. Mater.* **2006**, *18*, 2389.
(13) Shih, P. I.; Chien, C. H.; Wu, T. I.; Shu, C. F. *Adv. Funct. Mater.* **2007**, *17*, 3514.
(14) Vecchi, P. A.; Padmaperuma, A. B.; Qiao, H.; Sapochak, L. S.; Burrows, P. E. *Org. Lett.* **2006**, *8*, 4211.
(15) Cai, X. Y.; Padmaperuma, A. B.; Sapochak, L. S.; Vecchi, P. A.; Burrows, P. E. *Appl. Phys. Lett.* **2008**, *92*, 083308.
(16) Burrows, P. E.; Padmaperuma, A. B.; Sapochak, L. S.; Djurovich, P.; Thompson, M. E. *Appl. Phys. Lett.* **2006**, *88*, 183503.
(17) Shih, P. I.; Chiang, C. L.; Dixit, A. K.; Chen, C. K.; Yuan, M. C.; Lee, R. Y.; Chen, C. T.; Diau, E. W. G.; Shu, C. F. *Org. Lett.* **2006**, *8*, 2799.
(18) Wong, K. T.; Chen, Y. M.; Lin, Y. T.; Su, H. C.; Wu, C. C. *Org. Lett.* **2005**, *7*, 5361.
(19) Yeh, S. J.; Wu, M. F.; Chen, C. T.; Song, Y. H.; Chi, Y.; Ho, M. H.; Hsu, S. F.; Chen, C. H. *Adv. Mater.* **2005**, *17*, 285.
(20) Tsai, M. H.; Lin, H. W.; Su, H. C.; Ke, T. H.; Wu, C. C.; Fang, F. C.; Liao, Y. L.; Wong, K. T.; Wu, C. I. *Adv. Mater.* **2006**, *18*, 1216.
(21) Zhang, X. J.; Jiang, C. Y.; Mo, Y. Q.; Xu, Y. H.; Shi, H. H.; Cao, Y. *Appl. Phys. Lett.* **2006**, *88*, 051116.
(22) Su, S. J.; Sasabe, H.; Takeda, T.; Kido, J. *Chem. Mater.* **2008**, *20*, 1691.
(23) Tsai, M. H.; Hong, Y. H.; Chang, C. H.; Su, H. C.; Wu, C. C.; Matoliukstyte, A.; Simokaitiene, J.; Grigalevicius, S.; Grazulevicius, J. V.; Hsu, C. P. *Adv. Mater.* **2007**, *19*, 862.
(24) Tokito, S.; Iijima, T.; Suzuri, Y.; Kita, H.; Tsuzuki, T.; Sato, F. *Appl. Phys. Lett.* **2003**, *83*, 569.
(25) Lei, G. T.; Wang, L. D.; Duan, L.; Wang, J. H.; Qiu, Y. *Synth. Met.* **2004**, *144*, 249.
(26) Holmes, R. J.; Forrest, S. R.; Tung, Y. J.; Kwong, R. C.; Brown, J. J.; Garon, S.; Thompson, M. E. *Appl. Phys. Lett.* **2003**, *82*, 2422.
(27) Brunner, K.; van Dijken, A.; Borner, H.; Bastiaansen, J. J. A. M.; Kiggen, N. M. M.; Langeveld, B. M. W. *J. Am. Chem. Soc.* **2004**, *126*, 6035.
(28) Williams, E. L.; Haavisto, K.; Li, J.; Jabbour, G. E. *Adv. Mater.* **2007**, *19*, 197.
(29) Yang, X. H.; Wang, Z. X.; Madakuni, S.; Li, J.; Jabbour, G. E. *Adv. Mater.* **2008**, *20*, 2405.
(30) Ren, X. F.; Li, J.; Holmes, R. J.; Djurovich, P. I.; Forrest, S. R.; Thompson, M. E. *Chem. Mater.* **2004**, *16*, 4743.
(31) Shih, P. I.; Chien, C. H.; Chuang, C. Y.; Shu, C. F.; Yang, C. H.; Chen, J. H.; Chi, Y. *J. Mater. Chem.* **2007**, *17*, 1692.

Scheme 1. Synthetic Route of pDPFB[a]

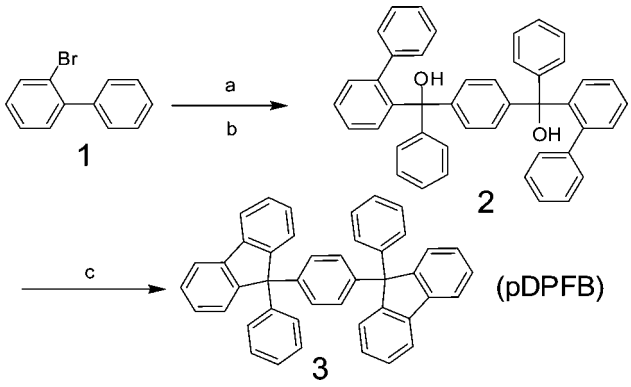

[a] Conditions: (a) BuLi, THF, −78 °C, 0.5 h; (b) pDPMB, −78 °C to rt; (c) HOAc, HCl, reflux for 10 h.

Fabrication and Characterization of OLEDs. pDPFB and mDPFB were synthesized and purified by thermal sublimation before use. The molecular structure of pDPFB was illustrated in Scheme 1. *N*,*N*′-Diphenyl-*N*,*N*′-bis(1-naphenyl)-1,1′-biphenyl-4,4′-diamine (NPB) and 2,9-dimethyl-4,7-diphenyl-1,10-phenanthroline (BCP) were purchased from Aldrich Chemical Co. and were purified by thermal sublimation, *N*,*N*′-dicarbazolyl-3,5-benzene (mCP) and FIr6 were purchased from Howe Electronic Colorant Limited and were used without further purification. In a general procedure, indium−tin oxide (ITO)-coated glass substrates were etched, patterned, and washed with detergent, deionized water, acetone, and ethanol in turn. All the organic layers were successively deposited by means of conventional vacuum deposition onto the ITO-coated glass substrates at a pressure of 8×10^{-5} Pa. In all devices, a cathode Ca:Ag layer with the weight ratio of 10:1 and a 100-nm-thick Ag capping layer were deposited through a 2-mm-diameter opening in a shadow mask. The active area of device was 5 mm^2. A quartz crystal oscillator placed near the substrate was used to monitor the thickness of each layer, which was calibrated ex situ using an Ambios Technology XP-2 surface profilometer. UV−vis absorption and fluorescence spectra were collected with a Hitachi U-3010 and Hitachi F-4500 spectrophotometer, respectively. EL spectra and chromaticity coordinates were measured with a SpectraScan PR650 photometer. Current density−voltage−luminance (*J*−*V*−*L*) measurements were made simultaneously using a Keithley 4200 semiconductor parameter analyzer and a Newport multifunction 2835-C optical meter, with luminance being measured in the forward direction. All device characterizations were carried out under ambient laboratory air at room temperature.

Synthetic Procedures of pDPFB. 2-Bromobiphenyl (3.495 g, 15 mmol) and THF (50 mL) were mixed and cooled to −78 °C, and then, *n*-BuLi (2.5 M in hexane, 6 mL, 15 mmol) was added dropwise. The whole solution was stirred at this temperature for 45 min followed by drop-adding a solution of 1,4-phenylenebis(phenylmethanone) (pDPMB) (2.863 g, 10 mmol) in THF (70 mL). The resulting mixture was gradually warmed to ambient temperature and kept stirring for 12 h; after that, 50 mL saturated aqueous $NaHCO_3$ was added to quench the reaction. The mixture was extracted with CH_2Cl_2 (3 × 60 mL), and the combined organic layers were dried with $MgSO_4$ and filtered and evaporated under reduced pressure. The crude residue dissolved in acetic acid (100 mL) and a catalytic amount of aqueous HCl (12 N) was added, and then, the whole mixture was warmed to reflux for 12 h. After being cooled to room temperature, the mixture was condensed under reduced pressure. The crude residue was purified by recrystallization from toluene to afford 5.301 g of pure pDPFB, white solid (yield 95%). ^{1}H NMR (400 MHz, DMSO) δ (ppm): 7.90 (d, J = 7.44 Hz, 4H), 7.41−7.36 (m, 8H), 7.30−7.26 (m, 4H), 7.24−7.18 (m, 6H), 7.05−7.03 (m, 8H). ^{13}C NMR: 151.34, 146.02, 144.05, 140.25, 128.26, 128.09, 127.74, 127.55, 126.67, 126.46, 120.22, 65.26. Elemental anal. Calcd (%) for $C_{44}H_{30}$: C, 94.59; H, 5.41. Found: C, 94.68; H, 5.42. MALDI-TOF mass (*m*/*z*): calcd 558.2, found 558.1 (M^+).

Synthetic Procedures of mDPFB. The same synthetic procedure was followed except pDPMB was substituted with 1,3-phenylenebis(phenylmethanone) (mDPMB).Yield 5.305 g, 95%. ^{1}H NMR (400 MHz, DMSO), δ (ppm): 7.82 (d, J = 7.54 Hz, 4H), 7.64 (s, 1H), 7.42 (t, J = 7.54 Hz, 4H), 7.34−7.28 (m, 9H), 7.26−7.25 (m, 5H), 7.17−7.16 (m, 4H), 6.99−6.98 (m, 1H), 6.91 (d, J = 7.44 Hz, 2H). ^{13}C NMR: 151.73, 146.57, 146.23, 140.69, 131.32, 128.67, 128.17, 127.98, 127.14, 126.75, 126.11, 120.67, 66.03. EI-MS (*m*/*z*): calcd 558.2, found 558 (M^+). Elemental anal. Calcd (%) for $C_{44}H_{30}$: C, 94.59; H, 5.41. Found: C, 94.23; H, 5.45.

Results and Discussion

Synthesis and Characterization of pDPFB and mDPFB. Scheme 1 illustrates the chemical structures of pDPFB and mDPFB along with the corresponding synthetic route. We chose the fluorene unit as the building block for the following considerations: (i) fluorene possess large triplet energy gaps of 2.89 eV[31] and (ii) their deep HOMO levels that typically fall below the HOMO levels of the carbazole-based host materials; e.g., mCP has a HOMO energy of 5.9 eV.[8] To maximize the HOMO−LUMO energy gaps in the target compounds, we connect two fluorenyl units at the sp^3-hybridized C-9 carbon atom by an inert unit of benzene to effectively block conjugation between them, avoiding any π-conjugating substituent; thus, the individual unit's conjugation length and triplet energy should remained relatively unperturbed. Moreover, the resulting molecules have a bulky, sterically hindered tetrahedron molecular skeleton, which not only hinders their close packing and crystallization but also increases their molecular rigidity, leading to amorphous materials having pronounced morphological stability. Direct phenyl−phenyl linkage must be avoided since biphenyl has a triplet energy of 2.72 eV.[30] Spiro-fluorene is not a suitable host for blue phosphorescent OLEDs since its triplet energy is only 2.70 eV (459 nm) (for details, see Figure 4d). To synthesize structurally perfect and free of ketonic defect compounds,[32,33] we adopted a Friedel−Crafts cyclization route to generate fluorene instead of using fluorenone as the starting material. Lithium-halo exchange of **1** with *n*-butyllithium in THF at −78 °C, followed by quenching with 1,4-phenylenebis(phenylmethanone) (pDPMB), afforded the tertiary alcohol **2** in 98% yield. Treatment of **2** with HOAc/HCl under refluxing for 10 h afforded the resulting material **3** in 95% yield. Replacing pDPMB with 1,3-phenylenebis(phenylmethanone) (mDPMB) yields the corresponding target compound mDPFB. A high purity targeted compound was obtained and unambiguously confirmed by ^{1}H NMR, ^{13}C NMR, MALDI-TOF, or EI mass spectrometry and elemental analysis.

(32) Wu, Y. G.; Li, J.; Fu, Y. Q.; Bo, Z. S. *Org. Lett.* **2004**, *6*, 3485.
(33) Wu, Y. G.; Zhang, J. Y.; Fei, Z. P.; Bo, Z. S. *J. Am. Chem. Soc.* **2008**, *130*, 7192.

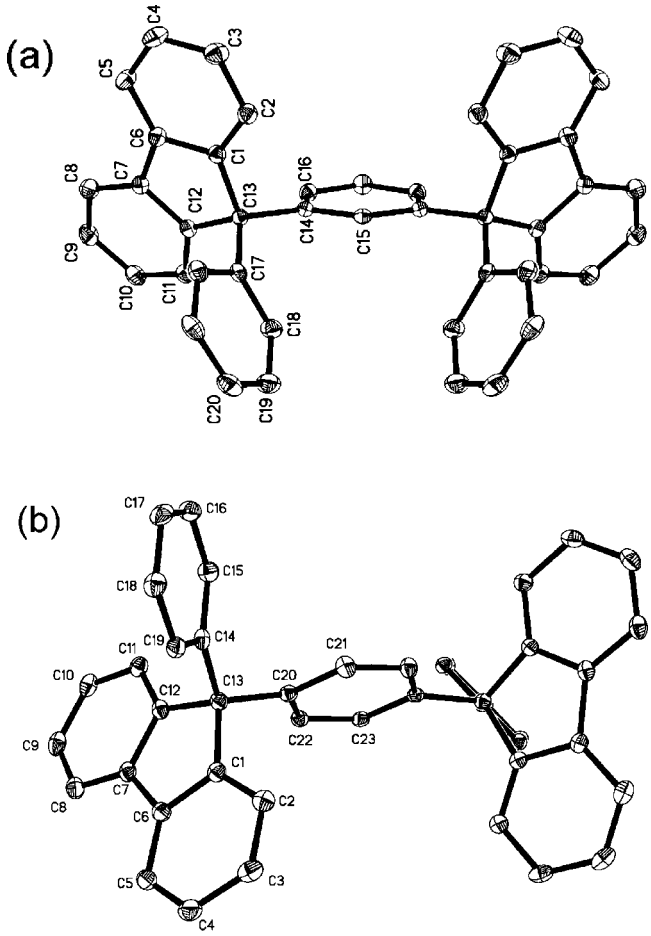

Figure 1. ORTEP drawing and related labeling scheme with 40% probability of thermal ellipsoids of mDPFB (a) and pDPFB (b).

Single Crystal X-ray Characterization and Molecular Packing Properties. For a better understanding of the structure−property relationship, we have carefully fostered a single crystal of mDPFB in toluene suitable for X-ray diffraction analysis. On average, each unit cell contains four mDPFB molecules and one toluene molecule. Figure 1a shows a Oak Ridge Thermal Ellipsoid Program (ORTEP) representation of the crystal structure of mDPFB; the whole molecule is highly symmetric with a symmetric mirror crossing C15 of the centric phenyl ring, while the two terminal fluorenyl rings and phenyl rings are arranged in tetrahedral structure with the fluorenyl ring and two phenyl rings are almost perpendicular to each other with a dihedral angle of 102.17° between the fluorenyl ring (C1−C13) and the phenyl ring (C17−C20), 117.04° between the phenyl ring (C17−C20) and the center phenyl ring (C14−C16), and 105.61° between the fluorenyl ring (C1−C13) and the phenyl ring (C17−C20). The two fluorenyl rings are almost planar with C13 protruding 0.12 Å from the plane of (C2, C5, C9, and C11), resembling those found in other substituted-fluorenes.[34] In the packing structure, the intermolecular distance between C3−H and C20 is 2.675 Å while that between C14−H and C21 is 2.291 Å. These values are all within the van der Waals radius, suggesting intermolecular interactions exist between the hydrogen atoms and the phenyl

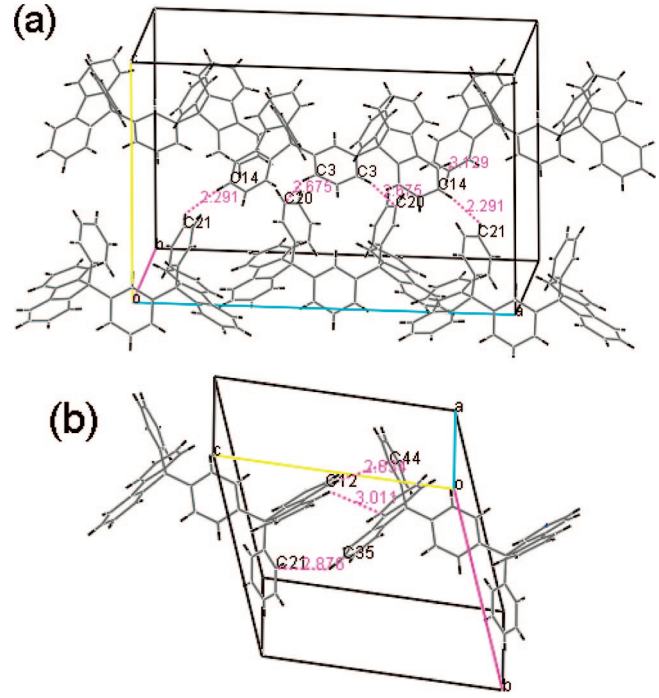

Figure 2. Molecular packing of mDPFB (a) and pDPFB (b) in one unit cell.

rings. Alternating interactions between the center phenyl rings and terminal phenyl rings and terminal phenyl rings to fluorenyl rings results in orthorhombic crystal system of mDPFB, containing four molecules in one unit cell. In this crystallography, no cofacial π-stacking is observed between fluorenyl rings and the minimum distance between them is 3.129 Å (edge C−H···C) which is longer than that of (C3−H···C20). This limits or eliminates an important mechanism of exciton transfer that can quench solid-state photoluminescence (PL) or shift its wavelength relative to isolated molecular behavior.[35]

As for pDPFB, it is more difficult to crystallize into a single crystal even though numerous efforts have been made. Fortunately, we got one after trial and error by diffusion of petroleum ether into a dichloromethane solution of pDPFB. Similarly, pDPFB also adopts a twisted tetrahedral structure with two phenyl rings, (C14−C19) and (C20−C23) are also perpendicular to the fluorenyl ring (C1−C12) with dihedral angles of 105.23° and 97.40°, respectively, while the two phenyl rings crossed with a 117.26° dihedral angle. Compared with mDPFB crystal structure, there is no symmetric mirror in the pDPFB crystal structure (for details, see Figure 1b). Moreover, the differences also revealed in the packing models of pDPFB in which two types of edge-to-face packing exist for the fluorenyl ring (C12−H) and phenyl ring (C21) to a neighboring unit, the phenyl ring (C44) or fluorenyl ring (C35−H), which are separated by distances of 2.831 and 2.876 Å, respectively (see Figure 2b). These types of packing take place in three directions along the three axes resulting in a triclinic crystal system of pDPFB. In this crystal system, no face-to-face interaction between fluorenyl rings was observed and the minimum distance (edge C−H to C) is

(34) Destri, S.; Pasini, M.; Botta, C.; Porzio, W.; Bertini, F.; Marchio, L. *J. Mater. Chem.* **2002**, *12*, 924.

(35) Wang, Z. X.; Shao, H. X.; Ye, J. C.; Zhang, L.; Lu, P. *Adv. Funct. Mater.* **2007**, *17*, 253.

Table 1. Physical Properties of mDPFB and pDPFB

compd	λ_{abs}[a] (nm)	λ_{PL}[b] (nm)	T_m, T_d[c,d] (°C)	E^{ox}_{onset} (V)	HOMO/LUMO$_{cal}$ $\Delta\varepsilon$ (eV)	ΔE (eV)
mDPFB	271, 307	313	93, 222, 354	1.79	6.2, 2.2	4.0
pDPFB	272, 308	313	not observed, >300, 386	1.53	6.0, 2.0	4.0

[a] Absorption maximum, measured in dichloromethane solution. [b] PL maximum, measured in dichloromethane. [c] Glass transition temperature. [d] Thermal decomposition temperature.

3.011 Å, similar to that observed in the mDPFB crystal. It is noteworthy that the driving forces of the molecular packing are the intermolecular C−H···π edge-to-face (between fluorenyl ring and phenyl ring) hydrogen-bond interactions rather than intermolecular $\pi-\pi$ electronic interaction between fluorenyl rings. These structural features may reduce the excimer formation in the solid state as already observed in ladder-type structures.[36−38]

Electrochemical Properties. In order to investigate the electrochemical behaviors of the target compounds, cyclic voltammetry (CV) measurements were performed in acetonitrile containing 0.1 M n-Bu_4NPF_6 as the supporting electrolyte versus a Ag/AgCl platinum disk as the working electrode and platinum wire as the counter electrode. The electrochemical data are summarized in Table 1. The anodic oxidation of pDPFB and mDPFB occurs in two waves with peaks E^1 at 1.64 and 1.89 V and E^2 at 1.90 and 2.01 V, respectively; the E^1 waves are quasireversible, while E^2 are irreversible. For pDPFB, the potential shift between E^1 and E^2 is around 0.25 V, whereas, for mDPFB, the shift between the two peaks is only 0.12 V. A comparison of the first oxidation peaks of mDPFB and pDPFB shows that pDPFB is more easily oxidized than the mDPFB unit. The positive shift of 0.25 V from pDPFB to mDPFB in the first oxidation may result from the electron-separating effect of the 1,3-disubstituted phenyl-linked fluorene, rendering the fluorenyl part of mDPFB more difficult to oxidize than that of the 1,4-disubstituted phenyl-linked florene of pDPFB. Or in other words, an extended π-conjugation between the π-electronic systems is preserved in the 1,4-disubstitued phenyl ring while that is blocked in the 1,3-disubsituted mDPFB. However, when comparing the second oxidation waves E^2 of mDPFB and pDPFB, there is only a 0.12 V potential difference. Such a small shift suggests that the substituent position on the center phenyl ring has little effect on the second oxidation wave.

The E^1 oxidation wave can be assigned to one-electron oxidation of the fluorenyl part on the C-9 position of the molecule, and the E^2 wave can be assigned to the oxidation of the phenyl-ring part of the fluorenyl units, as discussed in the literature.[36,39] Electrochemical data suggest that the substituent position of the central phenyl ring has little effect on the electrochemical properties of the phenyl-ring part, while it has some effect on the fluorenyl units.

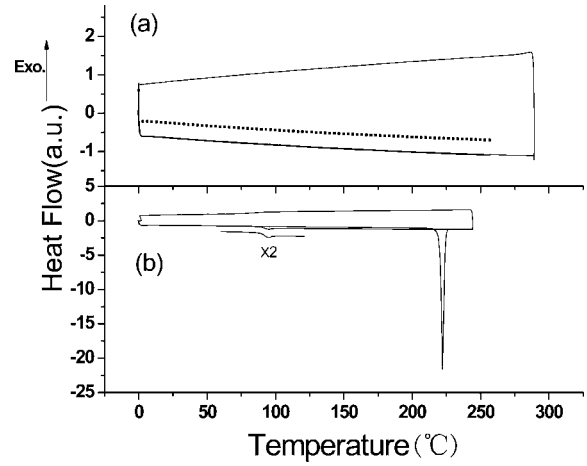

Figure 3. DSC curves of pDPFB (a) and mDPFB (b).

No distinct cathodic reduction process was recorded when applying the electrode potential sweep continuously between 0.0 and −3.0 V, which is different from spiro-flurene whose reduction potential lies at −2.7 V.[36] CV data also imply that these phenyl-substituted fluorenes are more favorable to oxidation rather than to reduction.

The HOMO and LUMO levels strongly depend on the electrochemical or redox properties of each individual component in the system. The HOMO or ionization potential (IP) was calculated using ferrocence (E_{FOC}) as the internal standard (which has a value of −4.8 eV relative to the vacuum level), while the E_{FOC} was calibrated to be 0.4 V versus the Ag/AgCl electrode. The HOMO energy levels were obtained according to the fellow equation: HOMO = $-(4.4 + E^{ox}_{onset})$ eV. These were 6.2 and 6.0 eV, for mDPFB and pDPFB, respectively. The LUMO energy levels were estimated by adding the optical band gaps to the HOMO energy values: these were 2.2 and 2.0 eV for mDPFB and pDPFB, respectively. Lower HOMO and higher LUMO energies of the host than the corresponding HOMO and LUMO (6.1 and 3.1 eV for FIr6) of the guest molecule is expected to favor carrier collection and recombination and exciton confinement, enabling efficient light emission.

Thermal Properties. Although similar in structure and electrochemical behavior, pDPFB and mDPFB are very different in thermal properties. The thermal properties of pDPFB and mDPFB were evaluated by thermogravimetric analyses (TGA) and differential scanning calorimetry (DSC) analyses. The glass transition (T_g), melting transition (T_m), and decomposition (T_d) temperatures are summarized in Table 1. As shown by the TGA curves (Supporting Information Figure S2), pDPFB and mDPFB were highly stable as they only started to decompose around 386 °C for pDPFB and around 354 °C for mDPFB. For comparison, mCP, which has been widely used as efficient building blocks within materials for OLEDs, starts to decompose around 280 °C. Thus, the higher thermal stability of the new DPFB building blocks appears to make these promising as host materials.

Figure 3a and b show the DSC heating curves of the two compounds. In the first heating of mDPFB, a very distinct endothermic peak due to melting was observed at 222 °C,

(36) Poriel, C.; Liang, J. J.; Rault-Berthelot, J.; Barriere, F.; Cocherel, N.; Slawin, A. M. Z.; Horhant, D.; Virboul, M.; Alcaraz, G.; Audebrand, N.; Vignau, L.; Huby, N.; Wantz, G.; Hirsch, L. *Chem.—Eur. J.* **2007**, *13*, 10055.
(37) Wong, K. T.; Chao, T. C.; Chi, L. C.; Chu, Y. Y.; Balaiah, A.; Chiu, S. F.; Liu, Y. H.; Wang, Y. *Org. Lett.* **2006**, *8*, 5033.
(38) Wong, K. T.; Chi, L. C.; Huang, S. C.; Liao, Y. L.; Liu, Y. H.; Wang, Y. *Org. Lett.* **2006**, *8*, 5029.
(39) Rault-Berthelot, J.; Granger, M. M.; Mattiello, L. *Synth. Met.* **1998**, *97*, 211.

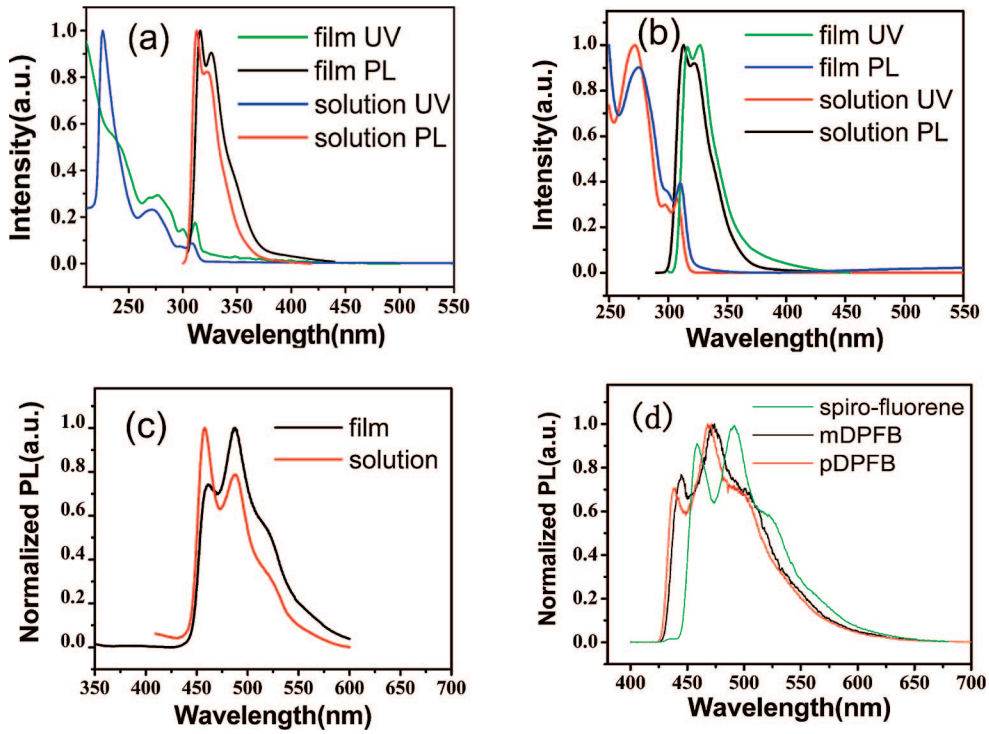

Figure 4. UV absorption and PL of pDPFB (a) and mDPFB (b), normalized PL of FIr6 in film and in dilute solution (c), and PL of spiro-fluorene, mDPFB, and pDPFB in dilute solution (2×10^{-5} M) at 77 K (d).

as shown in Figure 3b, but this behavior no longer existed upon subsequent cooling or heating scans; only a glass phase transition step occurred at 92 °C, higher than those of mCP (65 °C) or other silane-based UGHs (26−53 °C).[30,40] These facts indicate that mDPFB more favorably forms amorphous films rather than crystallizing upon thermal treatment and that an amorphous film can be achieved by conventional thermal vacuum deposition. However, things became very different when applying the DSC measurements over several cycles to the pDPFB, and no distinct endothermic or exothermic phase transition (including T_g or T_m) was detected in the range of 0−300 °C. We attempted several times to detect T_g using DSC, but no results were produce. However, T_g was not observed even after supercooling of the sample using liquid nitrogen at 300 °C. A similar behavior has also been observed for UGHs and similar bulky structures such as spiro-fluorene derivatives[41] and triphenylamine-substituted polyfluorene.[42] This phenomenon is probably due to the very bulky and rigid tetrahedron fluorenyl structure, hindering any segmental motion of the molecule even at elevated temperature up to 300 °C. Such thermal behavior would be expected to possess an enhanced thermal resistance to aggregation formation. Obviously, para-substituting can improve the rigidity of the molecule and thus improve the thermal stability. The excellent thermal properties with high T_d and T_g readily endow OLEDs with high thermal stability and thus high morphological stability, which is favorable to improving OLED performance and lifetime during operation.

Photophysical Properties. To investigate the photophysical properties, the UV−visible absorption and photoluminescent spectra (PL) of mDPFB and pDPFB were measured both in CH_2Cl_2 solution and in thin films (Figure 4). In solution, mDPFB exhibits three absorption bands located at around 271, 295, and 307 nm, coinciding with those of its parent fluorene, 9,9-diphenylfluorene, and confirming the rationale of our molecular design mentioned earlier. The strong absorption band at 271 nm can be assigned as the $\pi-\pi^*$ transition of the peripheral phenyl ring, and the weak band at 295 nm and the maximum band can be assigned to the fluorenyl part. The absorption spectrum of pDPFB also reveals similar patterns with three absorption bands centered at around 272, 296, and 308 nm. Upon UV excitation, mDPFB and pDPFB show almost identical fluorescent spectra with an intense peak at 313 nm and a shoulder at 322 nm, a little red-shift relative to UGHs (310 nm).[8] The singlet energy value is estimated to be approximately 4.0 eV, which is much higher than that of the FIr6 phosphor (E_T = 2.70 eV, 460 nm).

When carefully observing the UV−vis absorption and PL, we found that the Stoke shifts were only 6 and 5 nm, for mDPFB and pDPFB, respectively. Such small values recorded for mDPFB and pDPFB were consistent with the rigidity observed in the solid state structure.

When transfer from solution to the solid state, the absorption and fluorescence spectra of the target compounds are only red-shifted 3 and 4 nm for mDPFB and 2 and 3 nm for pDPFB, respectively, due to the presence of weak interactions between molecules (packing effect) in the solid state. The small bathochromic shift of the UV−vis absorption and PL observed

(40) Adamovich, V.; Brooks, J.; Tamayo, A.; Alexander, A. M.; Djurovich, P. I.; D'Andrade, B. W.; Adachi, C.; Forrest, S. R.; Thompson, M. E. *New J. Chem.* **2002**, *26*, 1171.
(41) Vak, D.; Lim, B.; Lee, S. H.; Kim, D. Y. *Org. Lett.* **2005**, *7*, 4229.
(42) Ego, C.; Grimsdale, A. C.; Uckert, F.; Yu, G.; Srdanov, G.; Mullen, K. *Adv. Mater.* **2002**, *14*, 809.

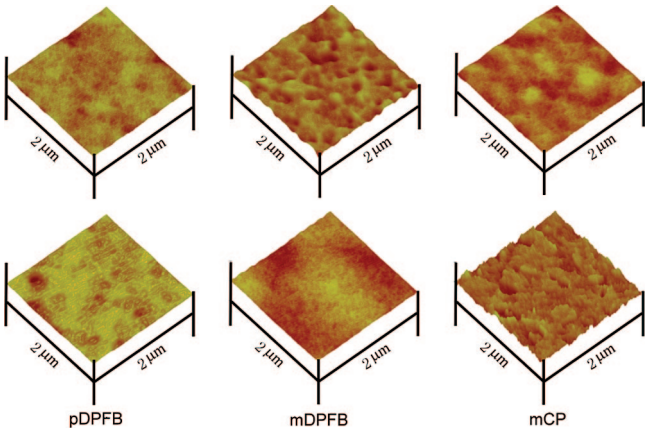

Figure 5. Tapping mode AFM image of pDPFB−mDPFB and mCP surface: (top) before heating; (bottom) after heating.

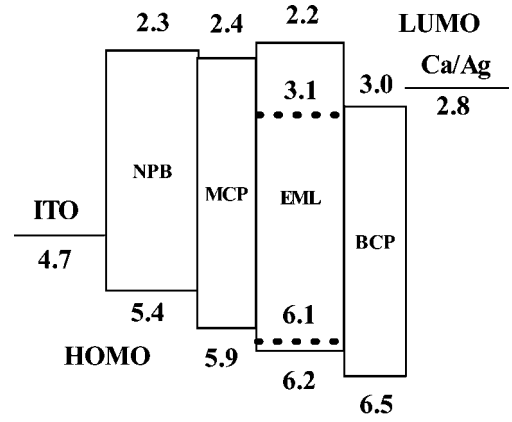

Figure 6. Schematic energy-level diagram of mDPFB devices. The HOMO and LUMO of the emitter are displayed by dashed lines.

in the solid state can also be explained by the crystal structure of mDPFB or pDPFB which shows a loose packing conformation (for details, see Figure 2a and b).

Figure 4d displays the phosphorescent spectra of mDPFB and pDPFB measured in a frozen 1,2-dichloroethane matrix at 77 K. The highest-energy 0−0 phosphorescent emission peak located at about 444 nm is taken for calculating the triplet energy gap of mDPFB, corresponding to 2.80 eV, while pDPFB has an emission centered at 438 nm, corresponding to 2.83 eV. These values were higher than those of FIrpic (2.62 eV) and FIr6 (2.70 eV). From these data, we would expect the energy transfer to FIr6 from both mDPFB and pDPFB to be effective and exothermic. Higher triplet energy of the host materials is a provision for effective confinement of the triplet excitons on the guest and for the consequential prevention of back energy transfer from the dopant to the host material.

Surface Morphology and Film-Forming Ability of mDPFB and pDPFB. In addition to the energy levels for the charge carrier injection, the surface morphology of the organic layer can also play an important role in determining the device performance. To get an insight into the contrasting behavior of the OLEDs, microstructural investigation for the pDPFB and mDPFB was performed. For comparison, we also fabricate and measured mCP film. Tapping mode atomic force microscope (AFM) imaging was carried out on four spots randomly chosen. Figure 5 shows AFM images of the pDPFB, mDPFB and mCP, all doped with 10% FIr6 by weight, before and after annealing on the ITO substrate, respectively. We observed a quite smooth surface of mCP on the coated ITO surface with a root-mean-square (rms) roughness of 6.37 nm measured over a 2 μm × 2 μm scan area. However, its surface became rather rough after annealing at 110 °C in N_2 after 10 h, and blocklike crystallites were formed, with an rms roughness of 16.88 nm. In contrast, the surface of pDPFB remained almost identical before and after annealing with rms values of 5.77 and 4.22 nm, respectively. No particle aggregation or phase-separation was observed, indicating the excellent miscibility of pDPFB with the dopant. As for mDPFB, however, it shows humble film-forming ability with an rms of 10.81 nm. Fortunately, its film-forming ability strengthened under the heating, with an rms of 3.61 nm, as shown in Figure 5. This fact indicates that pDPFB possesses very good film-forming ability, miscibility with the dopant, and morphological stability.

Electroluminescence Properties of Blue Phosphorescent OLEDs. To evaluate the electronic characteristics of the two new compounds mDPFB and pDPFB as host materials, we fabricate a series of devices using FIr6 as a blue phosphorescent dopant. We use ITO-coated glass as an anode and a thin layer of calcium coated with 100-nm-thick silver metals as a cathode; *N*,*N*′-di(naphthalene-1-yl)-*N*,*N*′-diphenylbenzidine (NPB) and 2,9-dimethyl-4,7-diphenyl-1,10-phenanthroline (BCP) serve as a hole transport layer and electron transport layer, respectively. The emitting layer (EML) is FIr6 doped into the mDPFB or pDPFB host, sandwiched in between NPB and BCP layers. Moreover, a thin layer of mCP was inserted between NPB and EML to confine excitons in the emissive layer and to reduce the energy barrier between the HOMO levels of NPB and EML, thereby facilitating resonant hole injection into the dopant (see the proposed device energy level scheme; Figure 6). A typical device configuration is ITO/NPB (40 nm)/mCP (15 nm)/EML (25 nm)/BCP (40 nm)/Ca:Ag (100 nm), where EML is either pDPFB doped with FIr6 at concentrations ranging from 5%, 8%, 10%, to 17% (by weight) for devices I, II, III, and IV or mDPFB doped with FIr6 at different concentrations ranging from 5%, 8%, to 10% for devices V, VI, and VII. The current density−luminance−voltage (*J*−*L*−*V*) curves and key characteristics of the devices are presented in Figure 7 and Tables 2 and 3.

Figure 7a shows the current density−voltage (*J*−*V*) curves of pDPFB devices. We can see that devices I, II, III, and IV show similar current density at the same driving voltage and almost identical turn-on voltages of about 6.5 V (for details, see Table 2), with no clear dependence on the dopant concentrations, sharply contrasting to UGH devices which show a dopant-concentration dependence of the current density. As for mDPFB devices, they also exhibit similar behavior like pDPFB devices with turn-on voltages between 6.3 and 7.6 V (see Figure 7c). This fact suggests that both pDPFB and mDPFB are active host materials which can conduct charge-carriers rather than an inert host material like UGHs. The differences between pDPFB and mDPFB devices are very weak as far as current density is concerned,

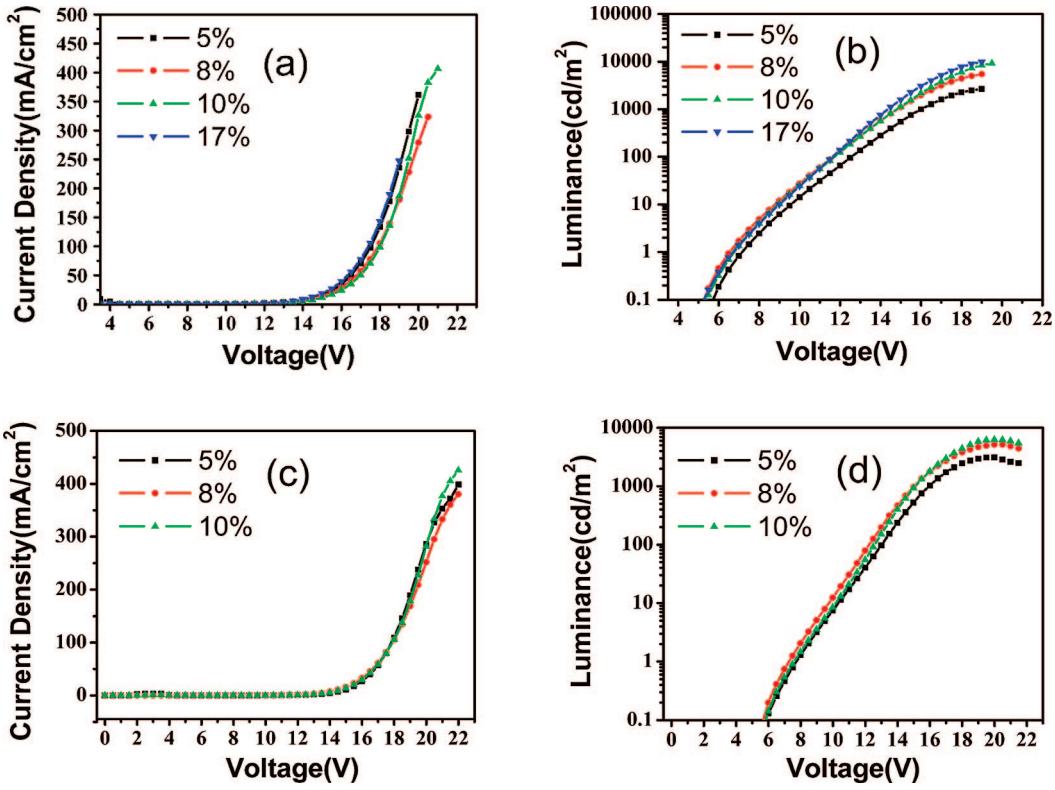

Figure 7. Current density versus voltage (a) and luminance versus voltage of pDPFB devices (b); mDPFB device characteristics (c and d): device structure ITO/NPB (40 nm)/mCP (15 nm)/EML (25 nm)/BCP (40 nm)/Ca:Ag (100 nm).

Table 2. Performance of Devices I−IV Based on pDPFB

properties	I	II	III	IV
turn-on voltage/V[a]	7.1	6.5	6.7	6.7
PE/lm/W[b]	0.6	1.2	2.6	2.0
LE/cd/A[b]	2.9	8.0	9.9	9.0
max brightness/cd/m^2[,c]	2659.7 (235.7)	5459.5 (180.3)	9269.2 (252.1)	9844.7 (247.3)
max PE/lm/W	0.9	16.4	18.9	7.8
max LE/cd/A	3.7	16.4	24.3	10.3
EL λ_{max}/nm[d]	460.0	460.0	460.0	460.0
CIE, x and y[d]	0.18, 0.29	0.18, 0.33	0.18, 0.33	0.18, 0.33

[a] At a brightness of 1 cd/m^2. [b] At 1000 cd/m^2. [c] The data in the parentheses are the corresponding current densities. [d] At 13 V.

Table 3. Performance of Devices V−VII Based on mDPFB

Properties	V	VI	VII	ref
turn-on voltage/V[a]	7.6	6.3	7.6	9.4
PE/lm/W[b]	0.8	1.2	1.4	1.2
LE/cd/A[b]	3.8	6.2	6.7	6.6
max brightness/cd/m^2	3098.9 (286.5)	5163.0 (295.5)	6284.1 (282.0)	9284.7 (402.1)
max PE/lm/W	1.4	2.0	2.1	1.3
max LE/cd/A	5.5	7.0	7.6	7.2
EL λ_{max}/nm	460.0	460.1	460.0	460
CIE, x and y[c]	0.19, 0.33	0.19, 0.33	0.19, 0.33	0.18, 0.30

[a] At a brightness of 1 cd/m^2. [b] At 1000 cd/m^2. [c] At 13 V.

indicating similar carrier conductivity. This is not difficult to understand because both molecules have the same building units and thus similar conductivity.

Figure 7b depicts the luminance−voltage ($L-V$) curves of pDPFB devices. Although devices I, II, III, and IV reveal similar turn-on voltages, device I shows lower luminance at the same applied voltages compared to the other three devices, while device IV displays the highest luminance. This suggests that increasing the doping concentration can improve the luminance of a device as energy transfer from the host to the dopant can be more complete and that a 5% doping concentration is not high enough. But further increase the doping concentration, e.g. 10% and beyond, the luminance improvement is not prominent, indicating a saturated doping concentration. Devices III and IV exhibit similar luminance with maximum luminance of 9269 and 9844 cd/m^2, respectively, at the current density of 252 and 247 mA/cm^2. As for mDPFB devices, they also show similar behavior, with devices VI and VII outperforming device V whose maximum luminance is 3098 cd/m^2 (at 286.5 mA/cm^2) compared to values 5163.0 (295.5) and 6284.1 (282.0) of devices VI and VII, respectively.

As can be seen from the luminous power efficiency dependence curves (see Figure 8), pDPFB devices behaved differently from mDPFB devices. The best performance can be ascribed to device III whose maximum luminous power efficiency η_{max} reached 18.9 lm/W and remains relatively high even at high luminance beyond 1000 cd/m^2. Device II also displays high efficiency with a maximum of 16.4, while device IV exhibits a moderate efficiency of 7.8 lm/W, but device I shows the lowest efficiency of 0.9 lm/W. Moreover, when the doping concentration reached 8%, the device efficiency improved by a factor of 2−9 compared to that at 5% doping. From the experimental data, we can infer the that optimal doping concentration for the pDPFB host and FIr6 dopant system is around 10%, while a lower or higher concentration ruins the efficiency. As mDPFB devices are concerned, however, the maximum efficiency is only 2.1 lm/W for device VII; this showed no prominent difference from device VI whose maximum is 2.0 lm/W, but outper-

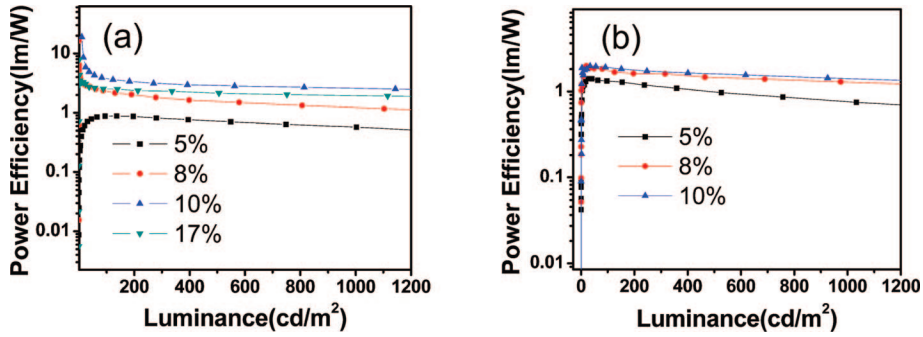

Figure 8. Efficiency versus luminance of pDPFB devices (a) and mDPFB devices (b).

formed device V whose value is 1.4 lm/W. But, the efficiency curves of all devices remain relatively flat even at high luminance, indicating low efficiency roll off.

For comparison purposes, we also fabricate another kind of device employing mCP, a commonly used phosphorescent host material in OLEDs, as the host material in the same device configuration: ITO/NPB (40 nm)/mCP (15 nm)/mCP: FIr6 (8%, 25 nm)/BCP (40 nm)/Ca:Ag (100 nm). The key characteristics are listed in Table 3 under the column heading ref. We found that the maximum luminous power efficiency is only 1.3 lm/W. Utilization of mCP and mDPFB as hosts showed similar efficiency, but the later showed lower turn-on voltage (9.4 versus 7.6 V). Compared with the mCP host, the pDPFB host decreased the turn-on voltage (6.7 V) and prominently elevated the device power efficiency to 18.9 lm/W, an over 10-fold improvement. In general, OLED performance is described as a product of four factors: (1) carrier balance factor, (2) exciton formation ratio, (3) photoluminescent quantum yield (PLQY), and (4) light out-coupling factor. Among them, there seem to be mainly two factors, 1 and 3, to determine these device performances. From the energy level point of view, mDPFB seems to have more ideal HOMO and LUMO levels than those of pDPFB, whose HOMO and LUMO are 6.0 and 2.0 eV, respectively, compared to 6.2 and 2.2 eV of mDPFB which are close to those of FIr6 (6.1 and 3.1 eV) and, however, show less performance. This is not difficult to understand because energy levels are not a direct factor to determine a device's performance, while the one direct factor is the carrier balance factor, which may be higher in pDPFB devices than in mDPFB devices, resulting from the bigger energy barrier for hole injection from mCP into the (mDPFB doped with FIr6) EML layer than into the (pDPFB doped with FIr6) EML layer. Another factor that determines a device's performance is PLQY (photoluminance quantum yield), and thus, we measured the relative PLQY of mDPFB and pDPFB films doped with 10% FIr6 and found that pDPFB films have higher PL intensity than mDPFB (for details, see Supporting Information Figure S3). Although we cannot measure the absolute PLQY values, the relative PL intensity sufficiently proves that pDPFB is more efficient than mDPFB in this host−dopant system. Moreover, pDPFB shows superior film-forming ability and miscibility with the dopant to mDPFB, witnessed by the morphological measurement, arising from its molecular structure, a twisted unsymmetrical tetrahedral structure, which has been discussed in the above section. In the solid state, pDPFB is inclined to form an amorphous,

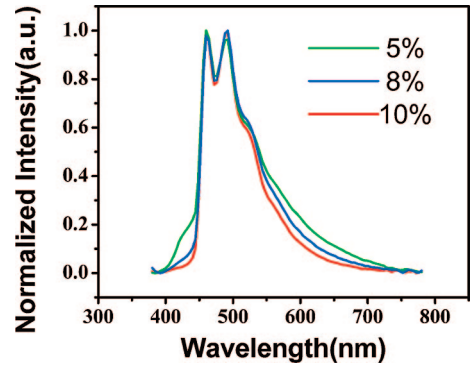

Figure 9. EL spectra of pDPFB devices at different doping concentrations.

homogeneous, and stable film rather than to crystallize, which is consistent with the difficulty of forming a single crystal. As for mCP devices, the higher HOMO energy level than that of FIr6 may not favor charge-carrier transfer effectively to the dopant, which has also been mention in the above section. Although mCP has higher triplet energy than that of pDPFB (2.90[26] versus 2.83 eV), it does not seem to be a dominant factor because both can effectively confine excitons on the FIr6 dopant (2.70 eV). Moreover, mCP is a hole-transporting material, which weakened the carrier balance and, thus, limited the device performance.[22] Furthermore, it shows humble film-forming ability, which is also disadvantageous to the device's performance. This explained why pDPFB devices exhibit the higher performance over those of mDPFB and mCP devices.

To explore the carrier-transporting and exciton-blocking properties, we also fabricated devices which consisted of only of a neat layer of mDPFB or pDPFB without doping phosphorescent emitter. A peak efficiency of 0.5 lm/W is obtained for both mDPFB and pDPFB devices, whose emission originated almost entirely from the NPB hole transport layer. This suggests that the devices show nonbalanced charge transport, with electron transport into the NPB layer where holes and electrons combine and form emitting excitons.

To fully understand the doping concentration effect on the EL spectrum, we recorded EL spectra of devices I, II, and III and presented the patterns in Figure 9. A small shoulder peak appears at about 440 nm in the EL spectrum, which becomes more apparent in devices whose doping level is lower than 5%. This phenomenon has also been observed previously in the UGH devices and is attributed to the

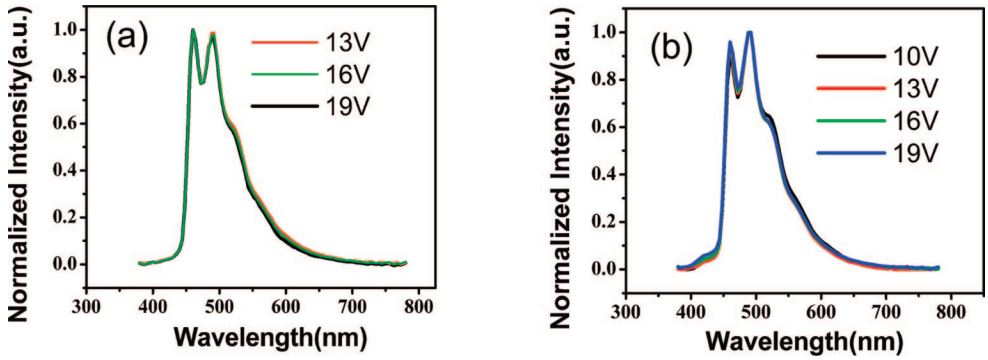

Figure 10. EL spectra of pDPFB device (a) and of mDPFB device (b) in a range of applied voltages.

emission of NPB, as a portion of the electrons injected from the cathode can overcome the barrier at the mCP/EML interface and enter into NPB, where they recombine with holes injected from the anode and form excitons.[8] At a doping level of 10% or beyond, the EL spectrum originated entirely from the FIr6 emitter, closely resembling the PL spectrum observed in its dilute solution, indicating complete energy transfer from the host to the dopant. But, further increasing the doping concentration results in intermolecular aggregation, T−T annihilation becomes prominent, and the luminous efficiency of the device decreased. On the basis of the above experimental data and analysis, we come to a conclusion that the optimal doping concentration is around 10% for pDPFB host and FIr6 dopant systems.

To explore the EL spectra stability, we record the spectra at different driving voltages. Figure 10 showed the EL spectra of pDPFB device III and mDPFB device VII, respectively, in a range of applied voltages. As shown in Figure 10, there is a main emission peak at 460 nm with a shoulder at 490 nm in the EL spectra of both pDPFB and mDPFB devices, which resembles the PL of FIr6 phosphorescent emitter in dilute solution. This suggests the same light-emitting process originating from the blue phosphorescent dopant FIr6. The EL spectra of both devices are independent of driving voltage in a range from 10 to 19 V, indicating balanced charge-carrier injection and transportation into the emissive layer. But, the shoulder peak of the mDPFB device is relatively stronger than that of the pDPFB device and the full-width at half-maximum (fwhm) of the mDPFB device (83 nm) is also very slightly larger than that of the pDPFB device (80 nm). Thus, the Commission Internationale de L′Eclairage coordinates of mDPFB devices are ruined, which have a CIE value of (0.19, 0.33) compared to (0.18, 0.33) of pDPFB devices. This behavior could originate from the conformational change of the dopant material in the excited state in both hosts.[43]

Conclusion

Two novel wide-energy-gap materials mDPFB and pDPFB based on fluorene have been designed and successfully synthesized via a Friedel−Crafts cyclization route. Two fluorenyl rings are connected through an inert core of benzene at the C-9 position of the sp^3 hybrid carbon, and each individual unit's photophysical and electronic properties are maintained by this connecting method. The comparative study on the single crystal structure shows that these novel molecules adopted a twisted tetrahedral structure and no face-to-face intermolecular $\pi-\pi$ interactions exist. This packing model avoids a red-shift of the spectrum and preserves the individual fluorenyl ring unit's conjugate length. Moreover, AFM surface morphology measurement results show that pDPFB possesses exceptional film-forming ability and morphology stability as well as solubility to the dopant. Photophysical and electrochemical property measurement results show that these two molecules have wide optical energy gaps of around 4.0 eV and higher singlet and triplet energies in addition to a matched energy level with the blue phosphorescent dopant, making them suitable for short-wave emitter host materials. Blue phosphorescent OLEDs were fabricated, and devices based on pDPFB show a high luminous power efficiency of 18.9 lm/W, indicating their potential use as a building block for developing new host materials for blue phosphorescent OLEDs. We demonstrate that very highly efficient blue phosphorescence can be achieved in the design of such host materials with high triplet energy and matched energy levels with the dopant, with good miscibility to the dopant, super film-forming ability, and thermal and morphological stability.

Acknowledgment. We acknowledge financial support from the National Natural Science Foundation of China (20825208, 60736004, 60671047, 50673093, and 20721061), the National Major State Basic Research Development Program (2006CB806203, 2006CB932103), the National High-Tech Research Development Program of China (2008AA03Z101), and the Chinese Academy of Sciences.

Supporting Information Available: Cyclic voltammograms of pDPFB and mDPFB in acetonitrile/Bu_4NPF_6 at a scan rate of 100 mV/s; thermal gravimetric analyses of pDPFB and mDPFB in N_2; X-ray crystallographic file (CIF). This material is available free of charge via the Internet at http://pubs.acs.org.

CM8032302

(43) Kim, M. S.; Choi, B. K.; Lee, T. W.; Shin, D.; Kang, S. K.; Kim, J. M.; Tamura, S.; Noh, T. *Appl. Phys. Lett.* **2007**, *91*, 251111.